PHILOSOPHICAL TRANSACTIONS OF THE ROYAL SOCIETY A

Phil. Trans. R. Soc. A (2010) **368**, 2765–2781
doi:10.1098/rsta.2010.0094

Influence of fatigue on the simulated relation between the amplitude of the surface electromyogram and muscle force

By Jakob L. Dideriksen, Dario Farina* and Roger M. Enoka

Center for Sensory-Motor Interaction (SMI), Department of Health Science and Technology, Aalborg University, Fredrik Bajers Vej 7 D-3, DK-9220 Aalborg, Denmark

A linear relation between surface electromyogram (EMG) amplitude and muscle force is often assumed and used to estimate the contributions of selected muscles to various tasks. In the presence of muscle fatigue, however, changes in the properties of muscle fibre action potentials and motor unit twitch forces can alter the relation between surface EMG amplitude and force. A novel integrative model of motor neuron control and the generation of muscle fibre action potentials was used to simulate surface EMG signals and muscle force during three fatigue protocols. The change in the simulated relation between surface EMG amplitude and force depended on both the level of fatigue and the details of the fatiguing contraction. In general, surface EMG amplitude overestimated muscle force when fatigue was present. For example, surface EMG amplitudes corresponding to 60 per cent of the amplitude obtained at maximal force without fatigue corresponded to forces in the range 10–40% of the maximal force across three representative fatigue protocols. The results indicate that the surface EMG amplitude cannot be used to predict either the level of muscle activation or the magnitude of muscle force when the muscle exhibits any fatigue.

Keywords: muscle fatigue; task failure; first dorsal interosseus; metabolites

1. Introduction

The surface electromyogram (EMG) amplitude is often used to estimate the level of force produced by the muscle in conditions when it is not possible to measure the force directly (Wang & Buchanan 2002; Bogey *et al.* 2005; Hoozemans & van Dieën 2005; Koo & Mak 2005; Staudenmann *et al.* 2007; Gatti *et al.* 2008). Such an application assumes a constant relation between surface EMG amplitude and muscle force. However, some of the determinants of EMG amplitude can change during tasks performed for relatively long durations. For example, both the force capacity and the electrophysiological membrane properties of the muscle fibres can change during fatiguing contractions, which will usually alter the relation between EMG amplitude and muscle force.

*Author for correspondence (df@hst.aau.dk).

One contribution of 13 to a Theme Issue 'The virtual physiological human: computer simulation for integrative biomedicine I'.

The amplitude of the twitch force produced by individual motor units decreases and the velocity of the contraction slows in the presence of fatigue (Thomas *et al.* 1991; Fuglevand *et al.* 1999). These types of adjustments alter the amount of activation required by the muscle to maintain a constant force. Moreover, the shapes of motor unit action potentials can change during fatiguing contractions (Dimitrova & Dimitrov 2003). The changes in motor unit twitch force and action potential shape will alter the EMG–force relation, which may become non-linear, as has been observed experimentally during contractions that are sustained at a constant force (de Luca 1984; Fuglevand *et al.* 1993*b*; Merletti & Lo Conte 1997; Carpentier *et al.* 2001). One of the hallmarks of the adjustments that occur during fatiguing contractions, however, is that they depend on the details of the task being performed (Enoka & Stuart 1992), which makes changes in the EMG–force relation difficult to predict experimentally.

Although several models of EMG generation and muscle force have been proposed (e.g. Fuglevand *et al.* 1992, 1993*a*; Baker & Lemon 1998; Duchêne & Hogrel 2000; Farina *et al.* 2004; Erdemir *et al.* 2007), most do not include time-varying parameters that can be used to simulate fatiguing contractions. We have recently proposed an integrative model of both surface EMG and force generation that includes the time-varying adjustments induced by fatigue (Dideriksen *et al.* 2009, submitted). This model provides a unique tool for inferring how EMG and muscle force change during different types of fatiguing contractions. The aim of the study was to investigate the influence of fatigue on the relation between EMG amplitude and muscle force using a set of models that describe the neural, muscular and contractile elements involved in performing a motor task.

2. Methods

The approach comprises the simulation of surface EMG signals in the presence of a progressive accumulation of intramuscular metabolites during a sustained contraction. The simulations were based on models that describe the activity of a population of motor neurons, the accumulation of metabolites within the muscle, and the generation of surface-recorded motor unit action potentials. The modelled muscle was the first dorsal interosseus, which is the muscle responsible for index finger abduction. These models have been described separately in previous work and are integrated in the current study to examine the influence of fatigue on the EMG–force relation. An overview of the main features of the simulation models is shown in figure 1, the key model parameters are stated in table 1 and the detailed equations for the model elements are reported in the appendix.

(*a*) *Metabolite concentration model*

The accumulation of metabolites in the muscle during sustained activity has a direct effect on the activation of muscle (Bigland-Ritchie *et al.* 1986; Gandevia 1998), the contractile properties of the muscle fibres (Fitts 1994; Allen *et al.* 2008) and the electrophysiological properties of the muscle fibre membranes (Dimitrova & Dimitrov 2003; Gazzoni *et al.* 2005). The simulation of metabolite

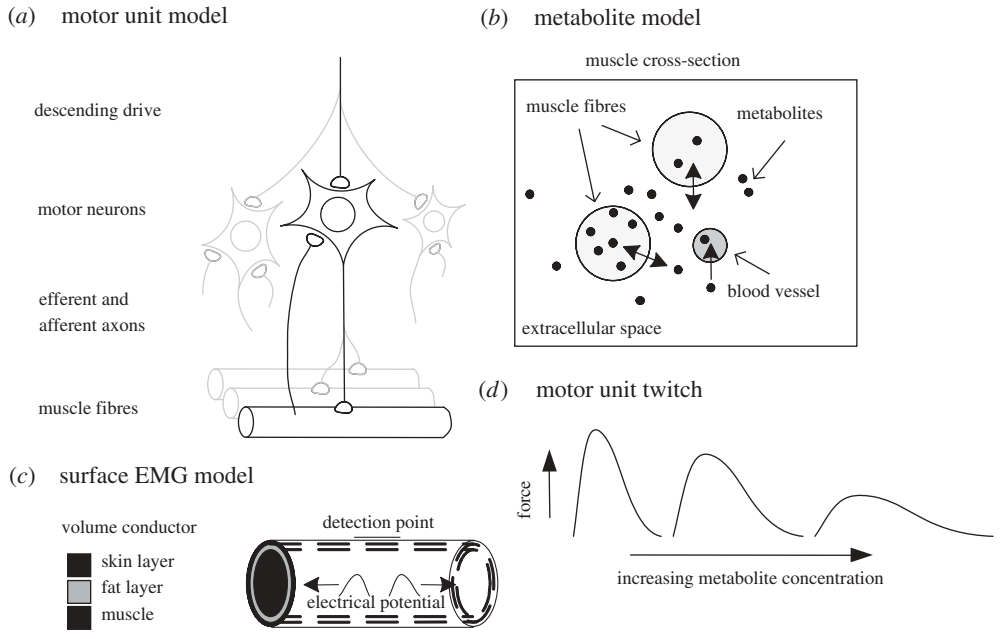

Figure 1. Schematic of the models used in the current study. (*a*) Inputs to the motor neuron pool (descending drive, excitatory and inhibitory afferent input) and innervated muscle fibres. (*b*) The model of the metabolite concentrations within the muscle. Metabolites are produced in the muscle fibres and diffuse across the cell membrane into the extracellular space, where they are removed in the blood stream. (*c*) The multi-layer volume conductor of the surface EMG model. (*d*) Example of the influence of an increase in intramuscular metabolite concentration on the twitch force of a motor unit.

Table 1. Model parameters and their assigned values. arb. units, arbitrary units, HO, intramuscular pressure at half blood-flow occlusion; HM, metabolite concentration at half maximal inhibition; MC_{ref}, reference metabolite concentration at the desired normalized change in tetanic force amplitude and relaxation time.

model parameter	assigned value
number of motor units, n	120
F_n/F_1 (arb. units)	80
V_0 (arb. units)	3
diffusion capacity, DC (arb. units)	0.01
removal capacity, RC (arb. units)	0.04
extracellular compartment volume, V_{EC} (arb. units)	1282
K_p	2×10^{-6}
K_i	2.5×10^{-4}
HO (arb. units, metabolite concentration)	30
HM (arb. units, metabolite concentration)	450
MC_{ref} (arb. units, metabolite concentration)	1150

concentrations was implemented as a compartment model of the metabolite dynamics in the intramuscular milieu (figure 1*b*; Dideriksen *et al.* submitted). As changes in metabolite concentrations are responsible for many of the adjustments

during a fatiguing contraction, the output of the metabolite model served as input to the other models to drive the adjustments that occurred during the simulated fatiguing contractions. Although the concentration of several metabolites is altered during fatiguing contractions (Allen *et al.* 2008), the model represents the net effect with one equivalent compound substance.

The metabolite model comprised one compartment for each motor unit ($n = 120$ in this study) and one compartment representing the extracellular space. The metabolite concentrations in each compartment were defined by the production (p), diffusion (d) and removal (r) of metabolites. Metabolite production occurred in each motor unit compartment and was related to the number of action potentials discharged by the motor unit. The diffusion of metabolites between each motor unit compartment and the compartment representing the extracellular space was determined by the concentration gradient between these compartments. The metabolites that diffused into the extracellular compartment were removed into the blood supply, with the removal rate being determined by the metabolite concentration in the extracellular compartment and the blood flow within the muscle. As blood flow was gradually occluded at high forces (Sjøgaard *et al.* 1988; Crenshaw *et al.* 1997), the magnitude of metabolite removal declined over time.

Equation (2.1) characterizes the differential equation for the intracellular metabolite concentration in each motor unit (MU; $\mathrm{MC_{MU}}$) and equation (2.2) specifies the extracellular metabolite concentration ($V =$ volume).

$$\frac{\mathrm{dMC_{MU}}}{\mathrm{d}t} = \frac{p_{\mathrm{MU}} - d_{\mathrm{MU}}}{V_{\mathrm{MU}}} \tag{2.1}$$

and

$$\frac{\mathrm{dMC_{EC}}}{\mathrm{d}t} = \frac{\sum d_{\mathrm{MU}} - r}{V_{\mathrm{EC}}}. \tag{2.2}$$

(*b*) *Motor neuron model and control algorithm*

The function of the motor neuron pool was based on a model developed by Fuglevand *et al.* (1993*a*). Based on the amplitude of the descending drive, the model computes the number of active motor units and the rate at which they discharge action potentials. The recruitment threshold for each motor unit is based on an exponential association between motor unit size and the net excitatory drive to the motor neuron pool, whereas the discharge rate after recruitment increases linearly with the increase in net excitatory drive up to a saturation limit (Fuglevand *et al.* 1993*a*).

To track a target force when the model parameters vary across time, the input to the model of the motor neuron pool was adjusted over time to minimize the error between the target force and the simulated force. The adjustment was accomplished with a PID control algorithm (equation (2.3)),

$$\mathrm{REI}(t) = K_p e(t) + K_t \int_1^t e(t)\mathrm{d}t + K_d(t)\frac{\mathrm{d}e(t)}{\mathrm{d}t}, \tag{2.3}$$

where REI denotes the required excitatory input to the motor neuron pool model to maintain the target force, e is the error in the simulated force relative to the target force, and K_p, K_i and K_d are the controller gains, which were chosen so that the tracking accuracy resembled experimental data (Jones *et al.* 2002; Dewhurst *et al.* 2007).

(*c*) *Neural adjustments during sustained contractions*

As motor units activated at the onset of a sustained contraction generally exhibit a decline in discharge rate, a target force is maintained by the progressive recruitment of additional motor units (Bigland-Ritchie *et al.* 1983; Garland *et al.* 1994; Carpentier *et al.* 2001; Mottram *et al.* 2005). The discharge rate of the newly recruited motor units initially increases, but then eventually also declines (Carpentier *et al.* 2001).

The instantaneous discharge rate of each motor unit was determined by the net synaptic input (NSI) to the motor neuron, which was the sum of the descending drive provided by the PID controller (DD), excitatory and inhibitory afferent inputs (EAI and IAI), and synaptic noise (SN). The EAI declines during fatiguing contractions, as indicated by a decline in the magnitude of the H-reflex (Duchateau *et al.* 2002), whereas the inhibitory afferent feedback increases as a function of metabolite concentration (Bigland-Ritchie *et al.* 1986). The net effect of these changes in afferent input to the motor neuron pool during a sustained contraction is a gradual decline in excitation, which must be compensated by an increase in descending drive to achieve the target force.

(*d*) *Muscular adjustments during sustained contractions*

The model for the isometric force produced by each motor unit was based on one developed by Fuglevand *et al.* (1993*a*), which was extended to a time-varying model. The force generated by each motor unit at a given discharge rate changes during fatiguing contractions that can be characterized by a decrease in force amplitude and an increase in contraction time (figure 1*c*). However, the magnitude of these changes varies with motor unit size (Thomas *et al.* 1991; Fuglevand *et al.* 1999). Equation (2.4) describes the shape of the simulated motor unit twitch (t): P denotes the force amplitude, T the contraction time, gain_f indicates a non-linear gain that depends on the discharge rate, and the two gain functions P_{g} and T_{g} alter the amplitude and contraction time of the motor unit twitch as a function of the metabolite concentration in its compartment,

$$t_{\mathrm{MU}}(t) = \mathrm{gain}_f \frac{P_{\mathrm{g_{MU}}}(\mathrm{MC_{MU}})Pt}{T_{\mathrm{g_{MU}}}(\mathrm{MC_{MU}})T} \mathrm{e}^{1-(t/(T_{\mathrm{g_{MU}}}(\mathrm{MC_{MU}})T))}. \tag{2.4}$$

(*e*) *Surface EMG*

The shape of a motor unit action potential changes during fatiguing contractions owing to modulation of the intracellular action potential and its velocity of propagation (Dimitrova & Dimitrov 2003). The changes in the shape of the single motor unit action potential as detected with a monopolar surface electrode are depicted for three motor units in figure 2.

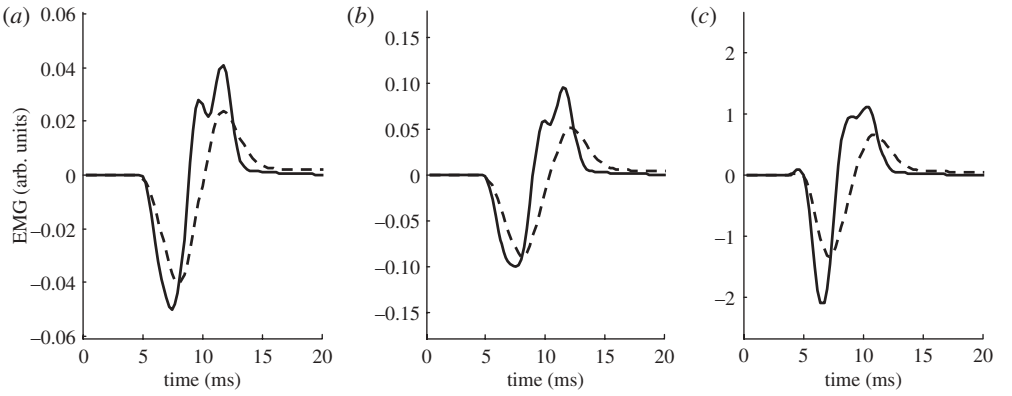

Figure 2. Single motor unit action potentials as recorded by a surface electrode in the absence of fatigue (propagation velocity $\approx 4.2\,\mathrm{m\,s^{-1}}$, solid line) and in the presence of muscle fatigue (propagation velocity $= 3\,\mathrm{m\,s^{-1}}$, dashed line) for (*a*) motor unit no. 1 (the smallest), (*b*) motor unit no. 60, and (*c*) motor unit no. 120 (the largest).

The surface EMG model involved the simulation of action potentials from a multilayer cylindrical volume conductor (Farina *et al.* 2004). The inner layer represented muscle, the next layer corresponded to subcutaneous tissue, and the outermost layer, on which the recording electrodes were placed, represented the skin. Based on the assigned thickness and conduction characteristics of each layer, a transfer function for the intracellular action potential at the detection point was computed. Changes in the surface-recorded action potential shape were characterized by 12 stages for the intracellular action potential, which were associated with changes in conduction velocity (Dimitrova & Dimitrov 2003).

Conduction velocity decreases with fatigue (Gazzoni *et al.* 2005; Klaver-kròl *et al.* 2007) and with the instantaneous discharge rate of the motor unit (Nishizono *et al.* 1989). The simulated conduction velocities, therefore, were determined from the combination of two functions that described these two effects (equation (2.5)): $\mathrm{MUCV_{DR}}$ defined the instantaneous value and $\Delta\mathrm{MUCV_{MC}}$ represented the percentage decrease from this value,

$$\mathrm{MUCV_{MU}}(t) = \mathrm{MUCV_{DR}}(\mathrm{DR_{MU}}(t))\mathrm{MUCV_{MC}}(\mathrm{MC_{EC}}(t)). \tag{2.5}$$

(*f*) *Simulation paradigms*

Three representative fatigue protocols were simulated. (i) Ramp contractions from 0 to 100 per cent maximum voluntary contraction (MVC; 17 s rise, 3 s pause) repeated for 380 s (19 ramps). The mean values for force and rectified EMG amplitude were obtained during each of the ramp contractions in epochs of 1 s and used to estimate the EMG–force relation. (ii) Two sustained contractions with an equivalent area under the force curve: 30 and 60 per cent MVC force sustained for 120 s and 60 s, respectively. After each sustained contraction, a 5 s pause was followed by a 20 s ramp contraction in which force was increased to the 100 per cent MVC value. The ramp contraction, which was also simulated in the absence of fatigue, was used to estimate the EMG–force relation before and after

the sustained contractions. (iii) Contractions with different target forces were sustained for longer than the time to task failure (20% MVC for 600 s; 35% MVC for 350 s; 50% MVC for 220 s; 65% MVC for 190 s; 80% MVC for 17 s). Task failure was defined as the point where the required excitatory input exceeded the maximal level, and therefore the target force could not be achieved. The EMG amplitudes during these contractions indicated changes in the EMG–force relation.

The surface EMG signals were simulated 10 times for each condition by randomly assigning the locations of the muscle fibres within the muscle, which corresponds to the variability that would be observed for measurements on different subjects.

3. Results

(*a*) *Simulation protocol 1*

Figure 3 depicts the simulated EMG and force traces for the first of the 19 ramp contractions in the first protocol and the change in the relation between the average rectified EMG amplitude and force during the 1st, 7th, 13th and 19th ramps is shown in figure 4*a*. The EMG–force curve is shifted to the left with increasing levels of fatigue, which means that EMG amplitude underestimated the level of force as fatigue developed in this protocol. For example, an EMG amplitude of 80 per cent MVC corresponded to approximately 65 per cent force during the first ramp contraction but to only approximately 45 per cent force during the 13th ramp.

Figure 4*b* depicts the number of single muscle fibre action potentials during the same four ramp contractions shown in figure 4*a*. Owing to the fatigue-induced slowing of the contraction time of the motor unit twitch, the target force is achieved with fewer action potentials in the 7th ramp than in the first (the curve is shifted to the right). In the 13th and 19th ramps, however, the amplitude of the motor unit twitch declined significantly and a greater number of action potentials were required to achieve the target force than in the first ramp (the curve is shifted to the left). Owing to changes in the shapes of the motor unit action potentials, near-maximal EMG amplitudes were achieved in the 7th and 13th ramps, even though the number of muscle fibre action potentials was only approximately 70 per cent of the maximal value in both cases.

(*b*) *Simulation protocol 2*

The second protocol involved contractions sustained at either 30 or 60 per cent MVC and then a ramp contraction to maximal force (figure 5*a*). Owing to the fatigue that developed in the simulated muscle, however, 100 per cent MVC was not achieved in the subsequent ramp contraction from which the EMG–force relations were derived (figure 5*b*). The EMG–force curves for the ramps following the 30 and 60 per cent MVC contractions are both shifted to the left relative to the non-fatigue curve; the effect is greater for the 30 per cent MVC contraction. The maximal EMG amplitude for the ramp contraction performed after the 60 per cent MVC task was approximately 6 per cent less than that for

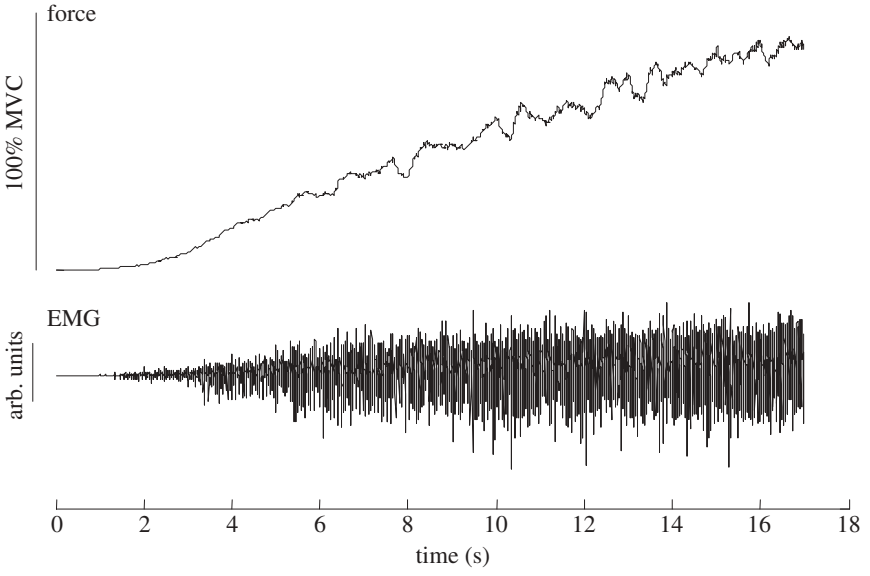

Figure 3. Simulated force and EMG during the first 17 s ramp contraction to maximum for the first protocol.

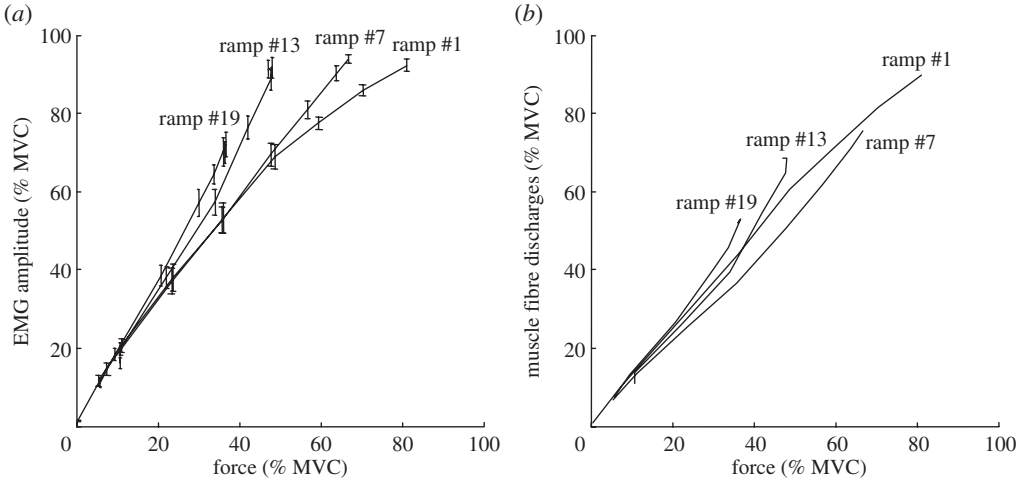

Figure 4. (*a*) Simulated relation between EMG and force during the 1st, 7th, 13th and 19th ramp contractions. Each contraction lasted 17 s and reached the maximal force at the end. Error bars indicate the variability in the EMG amplitude induced by different muscle fibre locations in the muscle. (*b*) Relation between force and number of single muscle fibre discharges (action potentials) during the 1st, 7th, 13th and 19th simulated ramp contractions.

the 30 per cent MVC task. The EMG–force relations after the two contractions differed by up to approximately 9 per cent of EMG amplitude at submaximal EMG amplitudes.

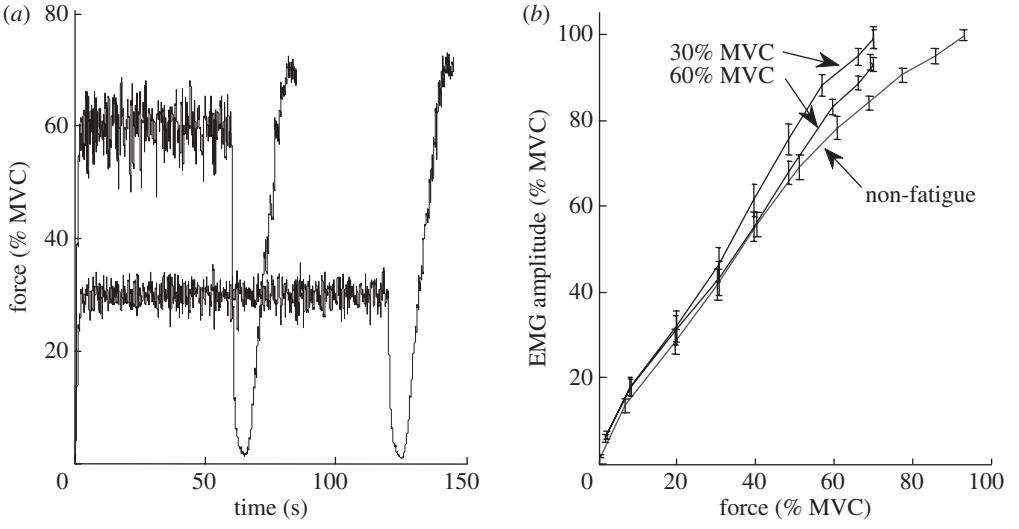

Figure 5. (*a*) The force traces for the two simulated contractions for the second protocol. The two contractions began with the force sustained at either 30% or 60% MVC for 120 s and 60 s, respectively. After a 5 s pause, the force was increased from 0% to 100% MVC in 20 s. Owing to the fatigue induced by the initial sustained contractions, the force did not reach 100% MVC. (*b*) The EMG–force relations determined from the ramp contractions at the end of each sustained contraction as well as one derived in the absence of fatigue ('non-fatigue').

(*c*) *Simulation protocol 3*

The third protocol involved five contractions sustained at different target forces beyond task failure (figure 6). The EMG amplitudes increased during the intervals when force was maintained at the target level, whereas both EMG amplitude and force decreased, but at different rates, when the target force could not be sustained any longer. The initial increase in EMG amplitude for the contractions less then 80 per cent MVC is due to the combined influence of an increased number of action potentials and an increase in the area of each action potential.

The simulations for the third protocol indicated that approximately 65 per cent of maximal EMG amplitude was achieved in contractions ranging from 20 per cent to 50 per cent force (figure 6). Moreover, EMG amplitude was not monotonically associated with force across the different conditions. For example, there were conditions under which EMG amplitude was greater at 20 per cent MVC force (e.g. at the time interval of approx. 60% with respect to the point of task failure) than at 35 per cent MVC force (e.g. at approx. 45% of the contraction duration).

(*d*) *Summary of the simulated EMG–force relations*

The simulated relations between EMG amplitude and force during the three protocols are summarized in figure 7. The dashed lines indicate the boundaries obtained from this set of simulations. The lower bound corresponds to the non-fatigue condition and can be approximated by a quadratic polynomial, where

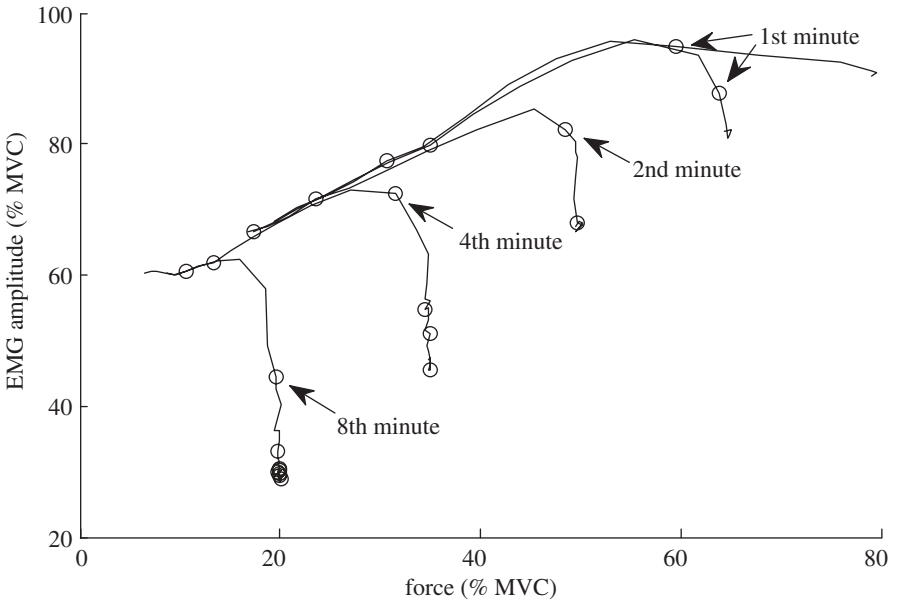

Figure 6. The relations between force and EMG amplitude in sustained contractions with target forces of 20% (bottom trace), 35%, 50%, 65% and 80% (top trace) MVC sustained beyond the point of task failure. The circles indicate each minute of simulated contraction time. The standard deviation for EMG amplitude due to different muscle fibre locations (not shown in figure) varied in the range 1–4% and was approximately 3% for all contraction levels beyond the point of task failure.

EMG and force (f) are expressed as percentages of MVC,

$$\mathrm{EMG} = -0.006f^2 + 1.6f. \tag{3.1}$$

The upper bound was derived from the task failure conditions and can be approximated by a linear polynomial, where EMG and force are expressed as percentages of MVC,

$$\mathrm{EMG} = 0.79f + 52.6. \tag{3.2}$$

Figure 7 indicates the large variability of the EMG–force relation when fatigue is present. For example, 60 per cent of EMG amplitude may correspond to forces that range from 10 per cent to 40 per cent MVC force.

4. Discussion

The aim of this study was to investigate the influence of muscle fatigue on the relation between surface EMG amplitude and muscle force. The results indicate that muscle fatigue substantially alters this relation by shifting the EMG–force curve to the left. The magnitude of the effect, however, depends on the task that was simulated and the level of fatigue experienced by the muscle. As the muscle fatigued, similar levels of EMG amplitude were observed for muscle forces that differed from each other by up to 40 per cent MVC force.

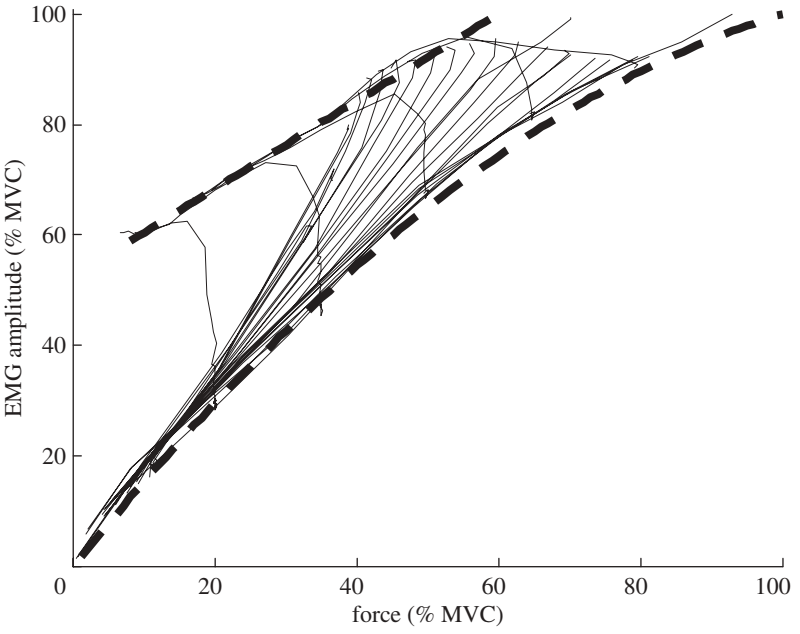

Figure 7. The relations between EMG amplitude and muscle force obtained from the entire set of simulations in the current study. Fatigue shifted the curve to the left. The magnitude of this shift depended on the task that was simulated and the level of fatigue experienced by the muscle. The dashed lines indicate the approximate bounds for the EMG–force relations. The density of curves between the two bounds indicates the difficulty in predicting the influence of fatigue.

In the non-fatigued muscle, the relation between EMG amplitude and force has been often reported as linear (Inman *et al.* 1952; Lawrence & de Luca 1983; Maluf *et al.* 2005). In the present simulations, however, the data were more accurately approximated with a quadratic polynomial (equation (3.2)), as has been observed experimentally (Day & Hulliger 2001). An increase in the EMG amplitude at constant force levels as simulated in the first and third protocols has been observed experimentally in the first dorsal interosseus muscle in several studies (Fuglevand *et al.* 1993*b*; Carpentier *et al.* 2001; Maluf *et al.* 2005). The trends in the EMG–force relation simulated in the third protocol before the point of task failure across contraction levels are similar to those reported by Fuglevand *et al.* (1993*b*). Moreover, the EMG amplitude has been shown to remain steady immediately after the force level begins to decline at task failure (de Luca 1984), as also predicted by the model; this phase is followed by a decline, described by the model and experimentally observed by Bigland-Ritchie *et al.* (1983).

Many physiological properties of the muscle (e.g. number of motor units, innervation number, range of peak discharge rates and motor unit synchronization) can influence the EMG–force relation (Fuglevand *et al.* 1993*a*; Yao *et al.* 2000; Keenan & Valero-Cuevas 2007). The relative significance of these parameters, however, is uncertain and surely varies between muscles (Keenan & Valero-Cuevas 2007) and with the type of contraction performed by the muscle (Keenan *et al.* 2009). Moreover, the presence of muscle fatigue further confounds the relation.

The current results indicate that it is not possible to predict with any accuracy the level of either muscle force or muscle activation in the presence of fatigue. Moreover, the change in the relation differed across the protocols used to induce fatigue, which reduces the possibility of compensating for the influence of fatigue with even a modelling approach. Several factors are responsible for the influence of task on the change in the EMG–force relation. For example, the rate of accumulation of metabolites in non-active motor units, and thereby their ability to produce force when recruited, depends non-linearly on the number of active motor units as well as on the extent to which blood flow is occluded. These effects were responsible for most of the differences between sustained constant-force contractions and intermittent ramp contractions. Furthermore, motor unit conduction velocity, which determines the shape of the action potential, depends on both metabolite concentrations and the instantaneous discharge rate, which varied across the fatigue protocols.

Consider, for example, the adjustments exhibited by moderate- and large-sized motor units during the second protocol. The motor units of moderate size are active during most of the 30 per cent MVC contraction and they experience a prolongation of twitch relaxation time that is greater than the decrease in the twitch amplitude (Thomas *et al.* 1991), which results in them being able to produce the same force at lower discharge rates. Conversely, larger motor units that are active during the 60 per cent MVC contraction experience a greater decrease in twitch force relative to the slowing of relaxation, which means that force declines at the same discharge rate. These two scenarios alter the EMG–force relation by influencing the EMG amplitude both directly (number of action potentials) and indirectly (change in the shape of the action potential).

In addition to being used to estimate muscle force, EMG amplitude is also often used as an indirect measure of the neural drive to the muscle during fatiguing contractions (St Clair Gibson *et al.* 2001; Ansley *et al.* 2004). As the results of the first protocol indicate, however, fewer muscle fibre action potentials are required to produce the target force during some fatiguing conditions despite the EMG amplitude remaining at its maximal level (ramp no. 7) and failed to represent the depression in the neural drive to the muscle. Although the magnitude of the neural drive and the EMG amplitude are partly associated, interpretations require caution (Farina *et al.* in press).

The findings in the current study, however, are based on a rather limited model of a functional neuromuscular system. The simulations are limited as several muscle parameters in the model were estimated indirectly by matching simulation results with previous experimental results (Dideriksen *et al.* submitted). Nonetheless, one advantage of such computational work is that it identifies gaps in knowledge that need to be addressed in subsequent experimental studies. For example, the simplified description of the metabolite accumulation includes only one metabolic compound substance, whereas several substances with different dynamics are responsible for muscle fatigue (Allen *et al.* 2008). The current knowledge within this field, however, does not allow precise modelling of all the metabolites and their interactions. Furthermore, the critical relation between the propagation velocity and the change in the shape of the intracellular action potential is not well described in the literature and is solely based on *in vitro* animal recordings. Finally, the model includes only one

muscle and is therefore unable to simulate the interplay between agonistic and antagonistic muscles. Despite these limitations, the main conclusions of the study are probably robust.

In conclusion, the presence of muscle fatigue significantly alters the relation between surface EMG amplitude and muscle force in a way that prevents the use of a simple scalar factor to compensate for the alteration of the EMG–force curve. The changes in the EMG–force curve indeed depend not only on the level of fatigue but also on the way in which fatigue is induced. Valid predictions of muscle force from the surface EMG, therefore, are not possible in contractions sustained long enough to induce muscle fatigue.

Appendix A

The appendix reports the model equations not presented in the main text and the parameter values used in the current study. The equations reported previously are not duplicated here; those related to the motor unit and isometric force models can be found in Fuglevand *et al.* (1993*a*) and Barry *et al.* (2007), and those for the EMG model can be found in Farina *et al.* (2004) and Dimitrova & Dimitrov (2003).

(*a*) *Metabolite concentration model*

In the following equations for the metabolite concentration model, t denotes time in 500 ms epochs.

$$\text{Volume of motor unit compartments: } V_{\mathrm{MU}} = V_0 + \mathrm{e}^{(\ln(F_n/F_2)/n)}\mathrm{MU}$$

and

$$\text{Metabolite production: } p_{\mathrm{MU}}(t) = V_{\mathrm{MU}}\mathrm{ND}_{\mathrm{MU}}(t),$$

where ND indicates the number of motor unit discharges in that epoch.

$$\text{Metabolite diffusion: } d_{\mathrm{MU}}(t) = \mathrm{DC}(\mathrm{MC}_{\mathrm{MU}}(t) - \mathrm{MC}_{\mathrm{EC}}(t))\, V_{\mathrm{MU}},$$

$$\text{Metabolite removal: } r_{\mathrm{MU}}(t) = \mathrm{RC}\,\mathrm{BF}(t)\mathrm{MC}_{\mathrm{EC}}(t)$$

and

$$\text{Intramuscular pressure: } \mathrm{IMP}(t) = \mathrm{IMP}_{\mathrm{ins}}(t) + \Delta\mathrm{IMP}(t),$$

where

$$\mathrm{IMP}_{\mathrm{ins}}(t) = 0.88f(t) + 10.65 \quad \text{and}$$

$$\Delta\mathrm{IMP}(t) = \sum_{x=1}^{t}\left(\tanh\left(\frac{f(x)-15}{8}\right)0.12\right)\left(\tanh\left(-\frac{f(x)-33}{3}\right)\frac{1}{2}+\frac{1}{2}\right)$$

and

$$\text{Blood flow: } \mathrm{BF}(t) = \tanh\left(-\frac{\mathrm{IMP}(t)-\mathrm{HO}}{4}\right)\frac{1}{2}+\frac{1}{2}.$$

(*b*) *PID control algorithm*

$$\text{Derivate gain:} K_d(t) = 1.6 \times 10^{-2}\, \mathrm{e}^{3.5\times 10^{-2}\mathrm{MMC}(t)} + 5.9 \times 10^{-2},$$

where MMC (mean metabolite concentration) is

$$\mathrm{MMC}(t) = \frac{\sum_{MU=1}^{n} \mathrm{MC}_{\mathrm{MU}}(t)}{\sum_{MU=1}^{n} V_{\mathrm{MU}}}.$$

(*c*) *Motor unit discharge rate*

$$\text{Net synaptic input:}\, \mathrm{NSI}_{\mathrm{MU}}(t) = \mathrm{DD}_{\mathrm{MU}}(t) + \mathrm{EAI}_{\mathrm{MU}}(t) + \mathrm{IAI}_{\mathrm{MU}}(t) + \mathrm{SN}_{\mathrm{MU}}(t),$$

$$\text{Descending drive (DD):}\, \mathrm{DD}_{\mathrm{MU}}(t) = k_{\mathrm{MU}}\mathrm{REI}_{\mathrm{MU}}$$

$$\text{and excitatory afferent input (EAI):}\, \mathrm{EAI}_{\mathrm{MU}}(t) = (1 - k_{\mathrm{MU}})\mathrm{REI}_{\mathrm{MU}} \sum_{x=1}^{t} \Delta HR(x),$$

where k_{MU} is

$$k_{\mathrm{MU}} = \frac{0.7\mathrm{REI}_{\mathrm{MU}} + 0.3\mathrm{RTE}_{\mathrm{MU}} - 0.3\mathrm{MDR}_{\mathrm{MU}}}{\mathrm{REI}_{\mathrm{MU}}}$$

and HR (H-reflex amplitude) is

$$\Delta\mathrm{HR}(t) = \mathrm{e}^{(t/(3\cdot 10^6/F(t)))} 0.4 \frac{-1}{3 \times 10^6/F(t)}, \quad F(t) > 0$$

and

$$\Delta\mathrm{HR}(t) = \frac{0.4}{3 \times 10^5}, \quad F(t) = 0.$$

$$\text{Inhibitory afferent input:}\, \mathrm{IAI}_{\mathrm{MU}} = \mathrm{IIM}_{\mathrm{MU}}(t)(E_{\max_{\mathrm{MU}}} - \mathrm{EIM}_{\mathrm{MU}}),$$

where IIM (inhibitory input magnitude) is

$$\mathrm{IIM}_{\mathrm{MU}}(t) = \tanh\left(\frac{\mathrm{MC}_{es}(t) - \mathrm{HM}}{\mathrm{HM}/2}\right)\frac{1}{2} + \frac{1}{2}$$

and EIM (maximal excitatory inhibition) is

$$\mathrm{EIM}_{\mathrm{MU}} = \mathrm{PDR}_{\mathrm{MU}} 0.78 - 14\frac{\mathrm{MU}}{n} + \mathrm{RTE}_{\mathrm{MU}} - \mathrm{MDR}_{\mathrm{MU}}$$

and

$$\text{Synaptic noise:}\, \mathrm{SN}_{\mathrm{MU}}(t) = \mathcal{N}\left(0, \frac{1}{6}\right)\sqrt{\mathrm{DD}_{\mathrm{MU}}(t)^2 + \mathrm{EAI}_{\mathrm{MU}}(t)^2 + \mathrm{IAI}_{\mathrm{MU}}(t)^2}.$$

(*d*) *Single motor unit force*

$$T_{g_{MU,MC}} = 1 + \left(1.66\frac{MU^2}{n} + 0.25\frac{MU}{n} - 0.25\right)\tanh\left(4\left(\frac{MC_{MU}}{MC_{ref}} - \frac{1}{2}\right)\right)\frac{1}{2} + \frac{1}{2},$$

$$P_{g_{MU}} = CF_{MU}\tanh\left(\left(\frac{MC_{MU}}{MC_{ref}} - h_{MU}\right)\frac{1}{0.5h_{MU}}\right)\frac{1}{2} + \frac{1}{2},$$

$$CF_{MU} = \frac{1}{Tg_{MU}}\left(1 + \left(\tanh\left(4\frac{MC_{MU}}{MC_{ref}} - \frac{1}{2}\right)\frac{1}{2} + \frac{1}{2}\right)\left(\frac{1}{b_{MU}} - 1\right)\right),$$

$$b_{MU} = 0.389\,e^{-4.413(MU/n)} + 0.935\,e^{0.182(MU/n)},$$

$$h_{MU} = \left(-2\frac{MU}{n} + 2.88\right)s_{MU}\,t_{MU}\,u_{MU},$$

$$s_{MU} = \tanh\left(\frac{MU - 0.75\cdot n}{0.34\cdot n}\right)1.04 + \tanh\left(-\frac{MU - 0.67n}{0.37n}\right)0.95 + 0.97,$$

$$t_{MU} = \left(\tanh\left(-\frac{MU}{0.12\cdot n} + 1\right)\right)13 + 1$$

and

$$u_{MU} = \left(\tanh\left(\frac{MU - n}{0.04\cdot n} + 1\right)\right)0.06 + 1.$$

(*e*) *Motor unit conduction velocity*

$$MUCV_{DR}(t) = 0.49\log(DR_i(t)) + 2.98$$

and

$$MUCV_{MC}(t) = \tanh\left(\frac{MC_{EC}(t)}{1100}\right)0.35.$$

References

Allen, D. G., Lamb G. D. & Westerblad H. 2008 Skeletal muscle fatigue: cellular mechanisms. *Physiol. Rev.* **88**, 287–332. (doi:10.1152/physrev.00015.2007)

Ansley, L., Schabort, E., St Clair Gibson, A., Lambert, M. I. & Noakes, T. D. 2004 Regulation of pacing strategies during successive 4-km time trials. *Med. Sci. Sports Exerc.* **36**, 1819–1825. (doi:10.1249/01.MSS.0000142409.70181.9D)

Baker, S. N. & Lemon, R. N. 1998 Computer simulation of post-spike facilitation in spike-triggered averages of rectified EMG. *J. Neurophysiol.* **80**, 1391–1406.

Barry, B. K, Pascoe, M. A., Jesunathadas, M. & Enoka, R. M. 2007 Rate coding is compressed but variability is unaltered for motor units in a hand muscle of old adults. *J. Neurophysiol.* **97**, 3206–3218. (doi:10.1152/jn.01280.2006)

Bigland-Ritchie, B., Johansson, B., Lippold, O. C., Smith, S. & Woods, J. J. 1983 Changes in motoneurone firing rates during sustained maximal voluntary contractions. *J. Physiol.* **340**, 335–346.

Bigland-Ritchie, B., Dawson, N. J. & Johansson, R. S. 1986 Reflex origin for the slowing of motoneurone firing rates in fatigue of human voluntary contractions. *J. Physiol.* **370**, 451–459.

Bogey, R. A., Perry, J. & Glitter, A. J. 2005 An EMG-to-force processing approach for determining ankle muscle forces during normal human gait. *IEEE Trans. Neural Syst. Rehabil. Eng.* **13**, 302–310. (doi:10.1109/TNSRE.2005.851768)

Carpentier, A., Duchateau, J. & Hainaut, K. 2001 Motor unit behaviour and contractile changes during fatigue in the human first dorsal interosseus. *J. Physiol.* **534**, 903–912. (doi:10.1111/j.1469-7793.2001.00903.x)

Crenshaw, A. G., Karlsson, S., Gerdle, B. & Friden J. 1997 Differential responses in intramuscular pressure and EMG fatigue indicators during low- vs. high-level isometric contractions to fatigue. *Acta Physiol. Scand.* **160**, 353–361. (doi:10.1046/j.1365-201X.1997.00168.x)

Day, S. J. & Hulliger, M. 2001 Experimental simulation of cat electromyogram: evidence for algebraic summation of motor-unit action-potential trains. *J. Neurophysiol.* **86**, 2144–2158.

de Luca, C. 1984 Myoelectric manifestations of localized muscular fatigue in humans. *CRC Crit. Rev. Bioeng.* **11**, 251–279.

Dewhurst, S., Graven-Nielsen, T., Vito, G. D. & Farina, D. 2007 Muscle temperature has a different effect on force fluctuations in young and older women. *Clin. Neurophysiol.* **118**, 762–769. (doi:10.1016/j.clinph.2006.12.006)

Dideriksen, J. L., Bækgaard, M., Farina, D. & Enoka, R. M. 2009 A model of the surface EMG amplitude at task failure. In *Proc. 39th Annual Meeting of the Society for Neuroscience, Chicago, IL, 17–21 October 2009*. Abstract 687.15/HH33.

Dideriksen J. L., Farina, D., Bækgaard, M. & Enoka, R. M. Submitted. An integrative model of motor unit activity during sustained submaximal contractions.

Dimitrova, N. A. & Dimitrov, G. V. 2003 Interpretation of EMG changes in fatigue: facts, pitfalls, and fallacies. *J. Electromyogr. Kinesiol* **13**, 13–36. (doi:10.1016/S1050-6411(02)00083-4)

Duchateau, J., Belastra, C., Carpentier, A. & Hinaut, K. 2002 Reflex regulation during sustained and intermittent submaximal contractions in humans. *J. Physiol.* **541**, 959–967. (doi:10.1113/jphysiol.2002.016790)

Duchêne, J. & Hogrel, J. Y. 2000 A model of EMG generation. *IEEE Trans. Biomed. Eng.* **47**, 192–201. (doi:10.1109/10.821754)

Enoka, R. M. & Stuart, D. G. 1992 Neurobiology of muscle fatigue. *J. Appl. Physiol.* **72**, 1631–1648.

Erdemir, A., McLean, S., Herzog, W. & van den Bogert, A. J. 2007 Model-based estimation of muscle forces excerted during movements. *Clin. Biomech.* **22**, 131–154. (doi:10.1016/j.clinbiomech.2006.09.005)

Farina, D., Mesin, L., Martina, S. & Merletti, R. 2004 A surface EMG generation model with multilayer cylindrical description of the volume conductor. *IEEE Trans. Biomed. Eng.* **51**, 415–426. (doi:10.1109/TBME.2003.820998)

Farina, D., Holobar, A., Merletti, R., Enoka, R. M. In press. Decoding the neural drive to muscles from the surface electromyogram. *Clin. Neurophysiol.*

Fitts, R. 1994 Cellular mechanisms of muscle fatigue. *Physiol. Rev.* **1**, 49–94.

Fuglevand, A. J., Winter, D. A., Patla, A. E. & Stashuk, D. 1992 Detection of motor unit action potentials with surface electrodes: influence of electrode size and spacing. *Biol. Cybern.* **67**, 143–153. (doi:10.1007/BF00201021)

Fuglevand, A. J., Winter, D. A. & Patla, A. E. 1993*a* Models of recruitment and rate coding organization in motor-unit pools. *J. Neurophysiol.* **70**, 2470–2489.

Fuglevand, A. J., Zackowski, K. M., Huey, K. A. & Enoka, R. M. 1993*b* Impairment of neuromuscular propagation during human fatiguing contractions at submaximal forces. *J. Physiol.* **460**, 549–572.

Fuglevand, A. J., Macefield, V. G. & Bigland-Ritchie, B. 1999 Force-frequency and fatigue properties of motor units in muscles that control digits of the human hand. *J. Neurophysiol.* **81**, 1718–1729.

Gandevia, S. C. 1998 Neural control in human muscle fatigue: changes in muscle afferents, moto neurones and moto cortical drive. *Acta Physiol. Scand.* **162**, 275–283. (doi:10.1046/j.1365-201X.1998.0299f.x)

Garland, S. J., Enoka, R. M., Serrano, L. P. & Robinson, G. A. 1994 Behavior of motor units in human biceps brachii during a submaximal fatiguing contraction. *J. Appl. Physiol.* **76**, 2411–2419.

Gatti, C. J., Doro, L. C., Langenderfer, J. E., Mell, A. G., Maratt, J. D., Carpenter, J. E., Hughes, R. E. 2008 Evaluation of three methods for determining EMG-muscle force parameters estimates for the shoulder muscles. *Clin. Biomech.* **23**, 166–174. (doi:10.1016/j.clinbiomech.2007.08.026)

Gazzoni, M., Camelia, F. & Farina, D. 2005 Conduction velocity of quiescent muscle fibers decreases during sustained contraction. *J. Neurophysiol.* **94**, 387–394. (doi:10.1152/jn.01182.2004)

Hoozemans, M. J. M. & van Dieën J. H. 2005 Prediction of handgrip forces using surface EMG of forearm muscles. *J. Electromyogr. Kinesiol* **15**, 358–366. (doi:10.1016/j.jelekin.2004.09.001)

Inman, V. T., Ralson, H. J., Saunders, J. B., Feinstein, B. & Wright, E. W. 1952 Relation of human electromyogram to muscular tension. *Electroencephalogr. Clin. Neurophysiol.* **4**, 187–194. (doi:10.1016/0013-4694(52)90008-4)

Jones, K. E., Hamilton, A. F. & Wolpert, D. M. 2002 Sources of signal-dependent noise during isometric force production. *J. Neurophysiol.* **88**, 1533–1544.

Keenan, K. G. & Valero-Cuevas, F. J. 2007 Experimentally valid predictions of muscle force and EMG in models of motor-unit function are most sensitive to neural properties. *J. Neurophysiol.* **98**, 1581–1590. (doi:10.1152/jn.00577.2007)

Keenan, K. G., Santos, V. J., Venkadesan, M. & Valero-Cuevas, F. J. 2009 Maximal voluntary fingertip force production is not limited by movement speed in combined motion and force tasks. *J. Neurosci.* **29**, 8784–8789. (doi:10.1523/JNEUROSCI.0853-09.2009)

Klaver-Król, E. G., Henriquez, N. R., Oosterloo, S. J., Klaver, P., Bos, J. M. & Zwarts, M. J. 2007 Distribution of motor unit potential velocities in short static and prolonged dynamic contractions at low forces: use of the within-subject's skewness and standard deviation variables. *Eur. J. Appl. Physiol.* **101**, 647–658. (doi:10.1007/s00421-007-0494-8)

Koo, T. K. K. & Mak, A. F. T. 2005 Feasibility of using EMG driven neuromusculoskeletal model for prediction of dynamic movement of the elbow. *J. Electromyogr. Kinesiol.* **15**, 12–26. (doi:10.1016/j.jelekin.2004.06.007)

Lawrence, J. H. & de Luca, C. J. 1983 Myoelectric signal versus force relationship in different human muscles. *J. Appl. Physiol.* **54**, 1653–1659.

Maluf, C. J., Jakobi, J. M., Semmler, J. G. & Enoka, R. M. 2005 Motor-unit activity differs with load type during a fatiguing contraction. *J. Neurophysiol.* **93**, 1381–1392.

Merletti, R. & Lo Conte, L. R. L. 1997 Surface EMG signal processing during isometric contractions. *J. Electromyogr. Kinesiol* **7**, 241–250. (doi:10.1016/S1050-6411(97)00010-2)

Mottram, C. J., Jakobi, J. M., Semmler, J. G. & Enoka, R. M. 2005 Motor-unit activity differs with load type during a fatiguing contraction. *J. Neurophysiol.* **93**, 1381–1392. (doi:10.1152/jn.00837.2004)

Nishizono, H., Kurata, H. & Miyashita, M. 1989 Muscle fiber conduction velocity related to stimulus rate. *Electroencephalogr. Clin. Neurophysiol.* **72**, 529–534. (doi:10.1016/0013-4694(89)90230-7)

Sjøgaard, G., Savard, G. & Juel, C. 1988 Muscle blood flow during isometric activity and its relation to muscle fatigue. *Eur. J. Appl. Physiol.* **57**, 327–335. (doi:10.1007/BF00635992)

Staudenmann, D., Daffertshofer, A., Kingma, I., Stegeman, D. F. & van Dieën, J. P. 2007 Independent component analysis of high-density electromyography in muscle force estimation. *IEEE Trans. Biomed. Eng.* **54**, 751–755. (doi:10.1109/TBME.2006.889202)

St Clair Gibson, A., Schabort, E.J. & Noakes, T. D. 2001 Reduced neuromuscular activity and force generation during prolonged cycling. *Am. J. Physiol.* **281**, R187–R196.

Thomas, C. K., Johansson, R. S. & Bigland-Ritchie, B. 1991 Attempts to physiologically classify human thenar motor units. *J. Neurophysiol.* **65**, 1501–1508.

Wang, L. & Buchanan, T. S. 2002 Prediction of joint moments using a neural network model of muscle activations from EMG signals. *IEEE Trans. Neural Syst. Rehabil. Eng.* **10**, 30–37. (doi:10.1109/TNSRE.2002.1021584)

Yao, W., Fuglevand, A. J. & Enoka, R. M. 2000 Motor-unit synchronization increases EMG amplitude and decreases force steadiness of simulated contractions. *J. Neurophysiol.* **83**, 441–452.